SIZE AND SHAPE EFFECTS ON STRENGTH AND ULTIMATE STRAIN IN FRP CONFINED RECTANGULAR CONCRETE COLUMNS

F.-Y. Yeh K.-C. Chang *

Department of Civil Engineering
National Taiwan University
Taipei, Taiwan 10617, R.O.C.

ABSTRACT

This paper is concerned with the effects of column size, carbon fiber-reinforced plastics (CFRP) volumetric ratio, column side to corner radius ratio and column side aspect ratio on the confinement efficiency of rectangular concrete columns confined with CFRP. The confined concrete nonlinear constitutive relationships are adopted which account for concrete under unequal lateral confining stresses under multi-axial stress conditions. A stiffness reduction procedure upon concrete cracking or crushing is also proposed. The finite element model is initially confirmed by comparing its numerical solutions with the experimental results for various parameters. The effects of above parameters on the peak strength and ultimate strain of the confined concrete are then parametrically studied. The test results and results of the parametric study indicate that the column axial compressive strength and ultimate strain increase with CFRP volumetric ratio, but decrease as the column side to corner radius ratio or the column side aspect ratio increases. For columns of a particular corner radius and CFRP volumetric ratio, the column axial compressive strength and ultimate strain decrease as column size and column side to corner radius ratio increases.

Keywords: CFRP, Strength of confined concrete, Ultimate strain, Shape effect and size effect.

1. INTRODUCTION

The advantages of CFRP include resistance against corrosion, their being lightweight, ease of cutting and use in construction, as well as their high strength and high elastic modulus. Therefore, CFRP has been extensively used in retrofitting and strengthening reinforced concrete structures, especially in regions of high seismic risk or high chloride corrosion. In the wake of recent earthquakes, such as the 1994 Northridge Earthquake (U.S.A.), the 1995 Kobe Earthquake (Japan) and the 1999 Chi-Chi Earthquake (Taiwan), CFRP composite material has become a popular alternative for seismic retrofit applications.

The results of many studies indicate, however, that FRP confined circular columns have better strength and ultimate strain than square or rectangular columns [1-3]. Previous studies of reinforced concrete members with arbitrarily shaped cross-sections without FRP wrapping have mostly focused on their ultimate strength [4]. Some constitutive models have also been proposed to predict the ultimate strength and strain of confined concrete with circular cross-sections [5,6]. A few studies of FRP wrapped circular reinforced concrete columns and rectangular reinforced concrete columns without FRP wrapping by using numerical method have focused on pre- and post-peak behavior and strength enhancement [7]. Recently, Wu and Wei [8] consider the effect of cross-sectional aspect ratio on the strength of CFRP-confined rectangular concrete columns by experimental study and propose a confined concrete strength model. Barrington *et al*. [9] investigate the impacts of corner radius on the development of hoop strains in the FRP wraps concrete columns. Elsanadedy *et al*. [10] focus on size effects of FRP-wrapped concrete columns by experimental and numerical investigation by using LS-DYNA software. In order to understand the differences among the failure mechanisms of FRP confined circular, square and rectangular columns, a nonlinear FEM model for FRP confined rectangular concrete columns has been developed and verified in an experimental study of 28 rectangular concrete column specimens with various parameters. Test results indicate that carbon fiber composite markedly increase the compressive strength and ultimate strain of concrete columns with rectangular cross-sections. The test results and the results of parametric studies also reveal that the axial compressive strength and ultimate strain of the column increase with the CFRP volumetric ratio (ρ_j), but decline as the column

* Corresponding author (ciekuo@ntu.edu.tw)

DOI : 10.1017/jmech.2012.118
Copyright © 2012 The Society of Theoretical and Applied Mechanics, R.O.C.
https://doi.org/10.1017/jmech.2012.118 Published online by Cambridge University Press

side to corner radius ratio (D/r) or the column side aspect ratio (B/D) increase. The axial compressive strength and ultimate strain of the columns of a particular corner radius (r) and CFRP volumetric ratio (ρ_j) fall as the column size (D) and the column side to corner radius ratio (D/r) increase.

2. NONLINEAR FINITE ELEMENT MODEL FOR FRP CONFINED RECTANGULAR CONCRETE COLUMNS

An FRP jacket, as opposed to a steel one which applies a constant confining pressure after yield, exhibits elastic behavior up to failure. Hence, a continuously increasingly confining action is expected. The amount of this action depends on the lateral dilation of concrete, which is determined by the confining pressure. As the compressive stress on the concrete increases, the concrete begins to crack internally and expand laterally, resulting in an apparent increase in Poisson's ratio. The confinement effect depends on the Poisson's ratio of the concrete. The Poisson's ratio of concrete is not a constant. This investigation utilizes the effect of the Poisson's ratio that was proposed by Kupfer *et al*. [11], allowing the lateral dilation of concrete and its interaction with the FRP jacket to be accounted for implicitly. The Poisson's ratio is expressed in the form,

$$\nu = \nu_0 \left[1.0 + 1.3763 \frac{\varepsilon_c}{\varepsilon_{co}} - 5.36 \left(\frac{\varepsilon_c}{\varepsilon_{co}} \right)^2 + 8.586 \left(\frac{\varepsilon_c}{\varepsilon_{co}} \right)^3 \right] \quad (1)$$

where ε_c = compressive strain and ε_{co} = compressive strain of unconfined concrete peak stress, respectively (generally ε_{co} = 0.002 can be assumed); v_0 = 0.2, the initial value of v.

The nonlinear finite element model, including the nonlinear constitutive relation for unequal lateral confining stresses, the multi-axial stress state of concrete, the composite failure criterion and the stiffness reduction following the cracking or crushing of concrete, is as follows.

2.1 Nonlinear Constitutive Relation for Unequal Lateral Confining Stresses

The starting point is a well-known stress-strain model for confined concrete that was proposed by Mander *et al*. [12], and has been extensively tested against experimental data. The model is based on the formula,

$$f_c = \frac{f'_{cc}\, xr}{r - 1 + x^r} \quad (2)$$

where

$$x = \frac{\varepsilon_c}{\varepsilon_{cc}} \; ; \quad \varepsilon_{cc} = \varepsilon_{co} \left[1 + 5 \left(\frac{f'_{cc}}{f'_{co}} - 1 \right) \right] \quad (2a,b)$$

$$r = \frac{E_c}{E_c - E_{\sec}} \; ; \quad E_{\sec} = \frac{f'_{cc}}{\varepsilon_{cc}} \quad (2c,d)$$

where f'_{cc} = compressive strength of confined concrete; f'_{co} = compressive strength of unconfined concrete; ε_{cc} = compressive strain at confined peak stress f'_{cc}, and E_c = Young's modulus for concrete.

Figure 1 presents the general solution to the multi-axial failure criterion in terms of two lateral confining stresses. The procedure for finding the ultimate strength ratio is rather complex so an iterative approach must be adopted. In this investigation an approximate equation that was proposed by Chang and Mander [13] is used to represent the failure surface that was identified by Mander *et al*. [12]. The equation is

$$K = \frac{f'_{cc}}{f'_{co}} = 1 + A\bar{x} \left(0.1 + \frac{0.9}{1 + B\bar{x}} \right) \quad (3)$$

with

$$\bar{x} = \frac{f'_{l1} + f'_{l2}}{2 f'_{co}} \quad (3a)$$

$$r = \frac{f'_{l1}}{f'_{l2}} \; , \; f'_{l2} \geq f'_{l1} \quad (3b)$$

$$A = 6.8886 - (0.6069 + 17.275r)\, e^{-4.989r} \quad (3c)$$

$$B = \frac{4.5}{\frac{5}{A}(0.9849 - 0.6306 e^{-3.8939r}) - 0.1} - 5 \quad (3d)$$

For a symmetric tri-axial state of stress $f_l = f_{l1} = f_{l2}$, the analytic confinement coefficient, K given by Mander *et al*. [12], is,

$$K = -1.254 + 2.254\sqrt{1 + 7.94\bar{x}} - 2\bar{x} \quad (4)$$

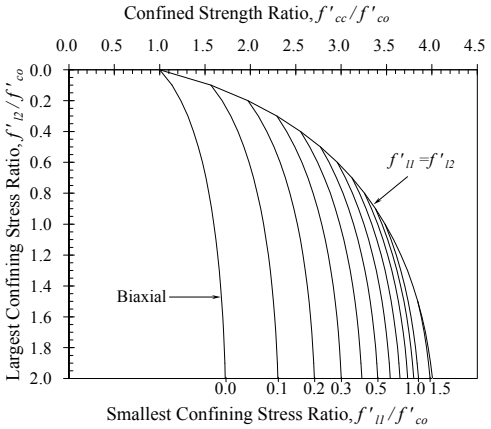


Fig. 1 Confined strength determination from lateral confining stresses for square and rectangular sections

https://doi.org/10.1017/jmech.2012.118 Published online by Cambridge University Press

2.2 Stress-Strain Relationships for Concrete and Composite Element

Concrete elements are used in the three-dimensional model of solids with or without reinforcing rebars. The solid element is capable of cracking under tension and crushing under compression. The stress-strain matrix $[D]_{rc}$ of such an element is defined as

$$[D]_{rc} = \left(1 - \sum_{i=1}^{N_r} V_i^R\right)[D_c] + \sum_{i=1}^{N_r} V_i^R [D_r]_i \tag{5}$$

where N_r = number of reinforcing materials; V_i^R = ratio of the volume of reinforcing material i to the total volume of the element; $[D_c]$ = stress-strain matrix for concrete, given by Eq. (6); and $[D_r]_i$ = stress-strain matrix for reinforcement i, given by Eq. (7).

The matrix $[D_c]$ is defined as

$$[D_c] = \frac{E_c}{(1+\nu)(1-2\nu)} \begin{bmatrix} (1-\nu) & \nu & \nu & 0 & 0 & 0 \\ \nu & (1-\nu) & \nu & 0 & 0 & 0 \\ \nu & \nu & (1-\nu) & 0 & 0 & 0 \\ 0 & 0 & 0 & \frac{(1-2\nu)}{2} & 0 & 0 \\ 0 & 0 & 0 & 0 & \frac{(1-2\nu)}{2} & 0 \\ 0 & 0 & 0 & 0 & 0 & \frac{(1-2\nu)}{2} \end{bmatrix} \tag{6}$$

where E_c = Young's modulus of concrete; v = Poisson's ratio of concrete.

The stress-strain matrix $[D_r]_i$ with respect to each coordinate system (x'_i, y'_i, z'_i) has the form

$$\begin{Bmatrix} \sigma^r_{xx} \\ \sigma^r_{yy} \\ \sigma^r_{zz} \\ \sigma^r_{xy} \\ \sigma^r_{yz} \\ \sigma^r_{xz} \end{Bmatrix} = \begin{bmatrix} E^r_i & 0 & 0 & 0 & 0 & 0 \\ 0 & 0 & 0 & 0 & 0 & 0 \\ 0 & 0 & 0 & 0 & 0 & 0 \\ 0 & 0 & 0 & 0 & 0 & 0 \\ 0 & 0 & 0 & 0 & 0 & 0 \\ 0 & 0 & 0 & 0 & 0 & 0 \end{bmatrix} \begin{Bmatrix} \varepsilon^r_{xx} \\ \varepsilon^r_{yy} \\ \varepsilon^r_{zz} \\ \varepsilon^r_{xy} \\ \varepsilon^r_{yz} \\ \varepsilon^r_{xz} \end{Bmatrix} = [D_r]_i \begin{Bmatrix} \varepsilon^r_{xx} \\ \varepsilon^r_{yy} \\ \varepsilon^r_{zz} \\ \varepsilon^r_{xy} \\ \varepsilon^r_{yz} \\ \varepsilon^r_{xz} \end{Bmatrix} \tag{7}$$

where E^r_i = Young's modulus of reinforcement material i.

The CFRP jacket is model as thin shell elements. The stress-strain matrix $[D]_{cf}$ used for composite material in the j-layer of a three-dimensional shell element is defined as [14],

$$[D]_{cf} = \begin{bmatrix} BE_{x,j} & B\nu_{xy,j}E_{x,j} & 0 & 0 & 0 & 0 \\ B\nu_{xy,j}E_{x,j} & BE_{y,j} & 0 & 0 & 0 & 0 \\ 0 & 0 & 0 & 0 & 0 & 0 \\ 0 & 0 & 0 & G_{xy,j} & 0 & 0 \\ 0 & 0 & 0 & 0 & \frac{G_{yz,j}}{f} & 0 \\ 0 & 0 & 0 & 0 & 0 & \frac{G_{xz,j}}{f} \end{bmatrix} \tag{8}$$

where

$$B = \frac{E_{y,j}}{E_{y,j} - (\nu_{xy,j})^2 E_{x,j}} \; ; \; f = Max\left\{ \begin{matrix} 1.2 \\ 1.0 + 0.2\frac{A}{25t^2} \end{matrix} \right\} \tag{8a,b}$$

where $E_{x,j}$ = Young's modulus in the x direction of layer j; $E_{y,j}$ = Young's modulus in the y direction of layer j; $v_{xy,j}$ = Poisson's ratio in the x-y plane of layer j; $G_{xy,j}$ = shear modulus in the x-y plane of layer j; $G_{yz,j}$ = shear modulus in the y-z plane of layer j; $G_{xz,j}$ = shear modulus in the x-z plane of layer j; A = area of each element in the layer plane; t = average thickness of shell element.

2.3 Multi-Axial Stress State Concrete and Composite Failure Criterion

The failure criterion of concrete due to a multi-axial stress state can be expressed in the form

$$\frac{F}{f'_{co}} - S \geq 0 \tag{9}$$

where F = a function of the principal stress state; S = failure surface; and f'_{co} = uniaxial compressive strength.

In the compression-compression-compression region ($0 \geq \sigma_1 \geq \sigma_2 \geq \sigma_3$), the failure criterion of Willam and Warnke [15] is applied. In this case, F takes the form

$$F = \frac{1}{\sqrt{15}}\left[(\sigma_1 - \sigma_2)^2 + (\sigma_2 - \sigma_3)^2 + (\sigma_3 - \sigma_1)^2 \right]^{1/2} \tag{10}$$

and S is defined as

$$S = \frac{2r_2(r_2^2 - r_1^2)\cos\eta + r_2(2r_1 - r_2)\left[4(r_2^2 - r_1^2)\cos^2\eta + 5r_1^2 - 4r_1 r_2\right]^{1/2}}{4(r_2^2 - r_1^2)\cos^2\eta + (r_2 - 2r_1)^2} \tag{11}$$

The terms used to define S are

$$\cos\eta = \frac{2\sigma_1 - \sigma_2 - \sigma_3}{\sqrt{2}\left[(\sigma_1 - \sigma_2)^2 + (\sigma_2 - \sigma_3)^2 + (\sigma_3 - \sigma_1)^2\right]^{1/2}} \tag{11a}$$

https://doi.org/10.1017/jmech.2012.118 Published online by Cambridge University Press

$$r_1 = a_0 + a_1\,\xi + a_2\,\xi^2 \tag{11c}$$

$$\xi = \frac{\sigma_h}{f'_{co}}, \quad \sigma_h = \frac{1}{3}(\sigma_1 + \sigma_2 + \sigma_3) \tag{11d,e}$$

If the failure criterion is satisfied in directions 1, 2 and 3, then cracking occurs in the planes perpendicular to the principal stresses σ_1, σ_2 and σ_3. If the failure criterion is satisfied in directions 1 and 2, then cracking occurs in the planes perpendicular to the principal stresses σ_1 and σ_2. If the failure criterion is satisfied only in direction 1, then cracking occurs in the plane perpendicular to the principal stress σ_1.

In this investigation, the Tsai-Wu failure criterion [16,17] is proposed for application to composite materials. Tsai and Hahn [16] introduced the strength index failure criterion in 1980 and then Tsai [17] introduced another strength ratio failure criterion in 1987. These are expressed as,

Strength index failure criterion

$$\zeta = A + B \tag{12}$$

Strength ratio failure criterion

$$\zeta = 1.0 \Big/ \left(-\frac{B}{2A} + \sqrt{(B/2A)^2 + 1.0/A} \right) \tag{13}$$

where ζ = the discriminant of the Tsai-Wu failure criterion and

$$A = -\frac{(\sigma_x)^2}{\sigma^f_{xt}\,\sigma^f_{xc}} - \frac{(\sigma_y)^2}{\sigma^f_{yt}\,\sigma^f_{yc}} - \frac{(\sigma_z)^2}{\sigma^f_{zt}\,\sigma^f_{zc}} + \frac{(\sigma_{xy})^2}{(\sigma^f_{xy})^2} + \frac{(\sigma_{yz})^2}{(\sigma^f_{yz})^2} + \frac{(\sigma_{xz})^2}{(\sigma^f_{xz})^2} + \frac{C_{xy}\,\sigma_x\,\sigma_y}{\sqrt{\sigma^f_{xt}\,\sigma^f_{xc}\,\sigma^f_{yt}\,\sigma^f_{yc}}} + \frac{C_{yz}\,\sigma_y\,\sigma_z}{\sqrt{\sigma^f_{yt}\,\sigma^f_{yc}\,\sigma^f_{zt}\,\sigma^f_{zc}}} + \frac{C_{xz}\,\sigma_x\,\sigma_z}{\sqrt{\sigma^f_{xt}\,\sigma^f_{xc}\,\sigma^f_{zt}\,\sigma^f_{zc}}} \tag{13a}$$

$$B = \left(\frac{1}{\sigma^f_{xt}} + \frac{1}{\sigma^f_{xc}}\right)\sigma_x + \left(\frac{1}{\sigma^f_{yt}} + \frac{1}{\sigma^f_{yc}}\right)\sigma_y + \left(\frac{1}{\sigma^f_{zt}} + \frac{1}{\sigma^f_{zc}}\right)\sigma_z \tag{13b}$$

where C_{xy}, C_{yz}, C_{xz} = coefficients of stress coupling effect in the $x-y$, $y-z$ and $x-z$ directions according to Tsai-Wu failure theory.

2.4 Stiffness Reduction Methodology

In this study, the finite element concrete model predicts elastic, cracking or crushing behaviour. If elastic behaviour is predicted, then the concrete is treated as a linear elastic material. If cracking or crushing behaviour is predicted, then the elastic stress-strain matrix is adjusted, as discussed below for one failure mode. Those for the other modes have been discussed elsewhere by Yeh and Chang [6].

The presence of a crack at an integration point is represented by a modification in the stress-strain relation by the introduction of a plane of weakness normal to the crack face. Also, a shear transfer coefficient β_t is introduced as a factor by which shear strength is reduced under subsequent loads that induce sliding across the crack face. The stress-strain relations of a material that has cracked in one direction only are,

$$[D^{ck}_c] = \frac{E_c}{(1+\nu)(1-2\nu)} \begin{bmatrix} 0 & 0 & 0 & 0 & 0 & 0 \\ 0 & \frac{1-2\nu}{1-\nu} & \frac{\nu(1-2\nu)}{1-\nu} & 0 & 0 & 0 \\ 0 & \frac{\nu(1-2\nu)}{1-\nu} & \frac{1-2\nu}{1-\nu} & 0 & 0 & 0 \\ 0 & 0 & 0 & \beta_t\frac{(1-2\nu)}{2} & 0 & 0 \\ 0 & 0 & 0 & 0 & \frac{(1-2\nu)}{2} & 0 \\ 0 & 0 & 0 & 0 & 0 & \beta_t\frac{(1-2\nu)}{2} \end{bmatrix} \tag{14}$$

where the superscript *ck* indicates that the stress strain relations are in a coordinate system that is parallel to principal stress directions with the x^{ck} axis perpendicular to the crack face.

If the material at an integration point fails under uniaxial, biaxial or triaxial compression, then this material is assumed to be crushed at that point. In a concrete element, crushing is defined as the complete deterioration of the structural integrity of the material (such as in material spalling). When crushing has occurred, material strength is assumed to have degraded to an extent that the contribution to the stiffness of an element at the integration point in question is reduced or neglected.

2.5 Analysis of FRP Confined Rectangular Concrete Columns Using Nonlinear FEM Model

Figure 2 presents a typical FRP confined rectangular concrete column and definitions of the geometric dimensions, where B = column width (length of longest side); D = column depth (length of shortest side); H = column height; r = corner radius and t_j = thickness of reinforcing FRP. The FRP volumetric ratio (ρ_j) of FRP confined rectangular concrete columns, is defined as

$$\rho_j = \frac{V_{\text{FRP}}}{V_{\text{concrete}}} = \frac{H\left[2(B-2r)+2(D-2r)+2\pi r\right]t_j}{H(B\times D - 4r^2 + \pi r^2)} = \frac{\left[2(N+1)(D/r)-(8-2\pi)\right]t_j}{\left[N(D/r)^2-(4-\pi)\right]r}; \quad \text{where } N = B/D \tag{15}$$

Because of the stress concentrations near the corner of FRP confined concrete columns, the finite model should make fine mesh at this area and the element size are limited by $r/10$ to $r/20$, in order to have suitable accuracy of numerical results. Figure 3 presents the

https://doi.org/10.1017/jmech.2012.118 Published online by Cambridge University Press

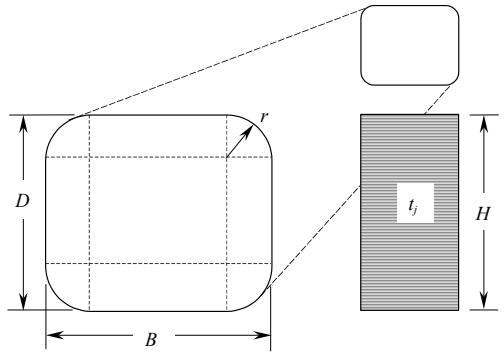
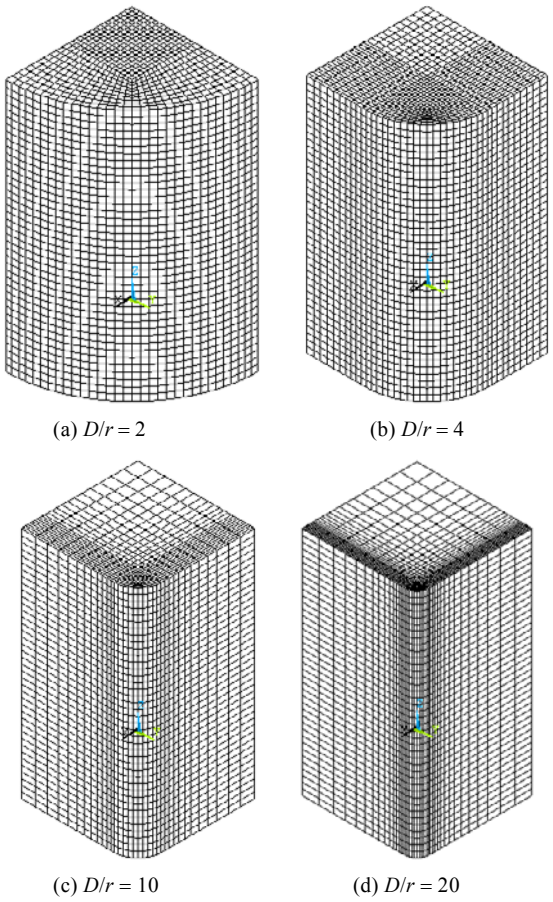


Fig. 2 Definitions of geometric dimension for FRP confined rectangular concrete columns



(a) $D/r = 2$ (b) $D/r = 4$

(c) $D/r = 10$ (d) $D/r = 20$

Fig. 3 Element mesh of nonlinear FEM model for FRP confined square concrete columns (B/D = 1) with different column side to corner radius ratio

element meshes of the nonlinear finite element model for FRP confined square concrete columns (B/D = 1) with various column side to corner radius ratios (D/r = 2, 4, 10 and 20). In a square section, the confining stress fields are different in the lateral directions because of stress concentration effects, and from Fig. 1, the different confining stress ratios in the two lateral directions result in different confined strengths of the FRP confined concrete. Accordingly, in this work, the different regions of the confined concrete are made from different materials with different strengths. In the FEM analysis, the concrete is then divided into various concrete materials $(f_c^m)_i$ according to the smallest $(f_{l1})_i$ and the largest $(f_{l2})_i$ confining stresses, as presented in Fig. 1, corresponding to the various confined strengths of concrete. Figure 4 presents the typical lateral confining stresses and material patterns.

The stress-strain characteristics of the confining mechanism are explicitly accounted for, while the lateral strain of the concrete is implicitly obtained via the interactive procedure that is presented in Fig. 5. The analysis can be performed in commercial computer software such as ABAQUS, ANSYS, MSC/NASTRAN and I-DEAS, among others. In this work, ABAQUS [18] is used and the element meshes of the nonlinear finite element model for confined rectangular concrete specimens are as presented in Fig. 3. Figure 6 presents the boundary conditions as $U_x(0, y, z) = 0$ in the $x = 0$ plane; $U_y(x, 0, z) = 0$ in the $y = 0$ plane; $U_z(x, y, 0) = 0$ in the $z = 0$ plane and $U_z(x, y, H/2) = (U_z)_i$ in the $z = H/2$ plane, corresponding to the ith step of incremental compressive axial strain $(\varepsilon_c)_i$ for displacement-controlled analyses. Figure 7 presents the flowchart of the analysis.

3. EXPERIMEMTAL PROGRAM

A total of 28 concrete columns of various dimensions were constructed and tested under axial compression to verify the proposed analytical procedure. The specimens are named according to the test parameters, which are column size, column side to corner radius ratio, number of CFRP layers and FRP type. For instance, Specimen S15-DR05-C2-200, has dimensions 15cm x 15cm × 30cm, D/r = 5, with two layers of FRP with FAW = 200g/m^2. Table 1 presents in detail the test matrix.

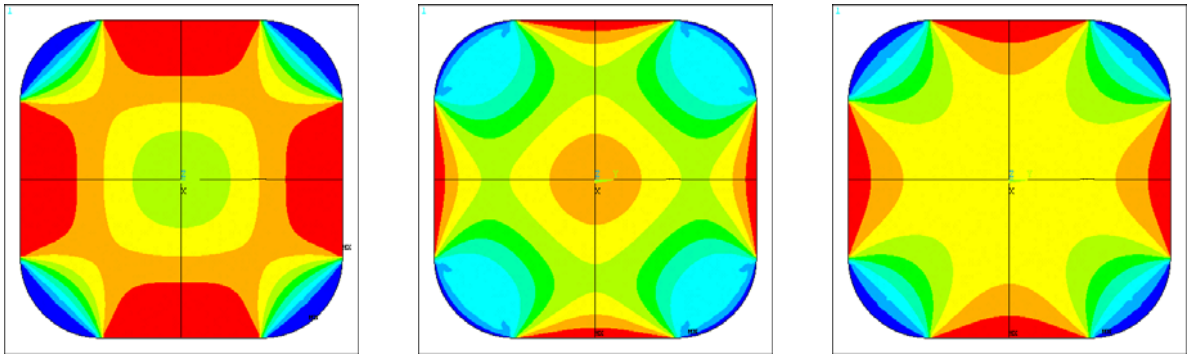
3.1 Preparation of CFRP Confined Concrete Specimens

The preparation of the specimen comprises two stages - making rectangular concrete columns and manually placing the CFRP around these columns. The manual layout procedure was as follows. A thin layer of primer epoxy was initially applied to the concrete surface. After the primer epoxy on concrete surface had been cured at the ambient temperature for several hours, a carbon fiber sheet was applied to the concrete columns. To fix the sheet and the other on top of the installed sheet, a paintbrush or rollers were used to ensure that the carbon fiber was saturated with epoxy. The excess epoxy used for each layer was squeezed out using a flat plastic scraper. The length of overlay exceeded 10cm, and each subsequent was applied at least one hours after the preceding layer. After all of the required sheet layers had been applied, the CFRP jacketing was cured under ambient conditions.

https://doi.org/10.1017/jmech.2012.118 Published online by Cambridge University Press

Table 1 The experimental parameters of 28 FRP confined concrete columns

Specimen	Concrete strength	Column width	Side length	Column height	Corner radius	Number of layer	FRP type	FRP volumetric ratio	amount
No.	f'_{co}	B	D	H	r		FAW	ρ_j	N
	MPa	cm	cm	cm	cm		g/m^2	%	set
S15-DR05-C2-200	20.6	15	15	30	3	2	200	0.56%	2
S15-DR05-C3-250	20.6	15	15	30	3	3	250	1.04%	2
S30-DR10-C3-250	20.6	30	30	60	3	3	250	0.53%	2
S30-DR10-C5-300	20.6	30	30	60	3	5	300	1.06%	2
S45-DR15-C4-300	20.6	45	45	90	3	4	300	0.57%	2
S45-DR15-C7-300	20.6	45	45	90	3	7	300	1.00%	2
R15-BD1.5-DR05-C2-250	20.6	22.5	15	45	3	2	250	0.58%	2
R15-BD1.5-DR05-C3-300	20.6	22.5	15	45	3	3	300	1.05%	2
R30-BD1.5-DR10-C3-300	20.6	45	30	90	3	3	300	0.53%	2
R30-BD1.5-DR10-C6-300	20.6	45	30	90	3	6	300	1.07%	2
R15-BD2.0-DR05-C2-250	20.6	30	15	60	3	2	250	0.53%	2
R15-BD2.0-DR05-C4-250	20.6	30	15	60	3	4	250	1.06%	2
R30-BD2.0-DR10-C4-250	20.6	60	30	120	3	4	250	0.54%	2
R30-BD2.0-DR10-C8-250	20.6	60	30	120	3	8	250	1.07%	2



(a) Smallest confining stress $(f_{l1})_i$ (b) Largest confining stress $(f_{l2})_i$ (c) $(f_c'^m)_i$ for different concrete material classified by $(f_{l1})_i$ and $(f_{l2})_i$

Fig. 4 Characteristic of FRP confined square concrete columns

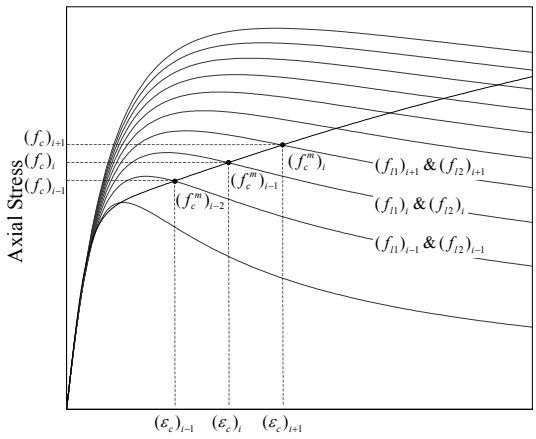


Fig. 5 Nonlinear finite element analysis concept and procedure for FRP confined rectangular concrete columns

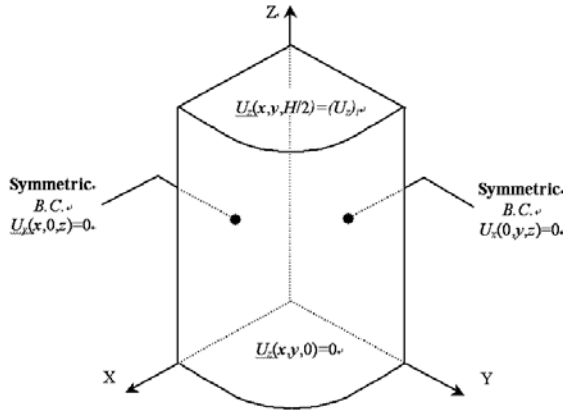


Fig. 6 Boundary conditions of one eighths FEM model for FRP confined rectangular concrete columns

https://doi.org/10.1017/jmech.2012.118 Published online by Cambridge University Press

3.2 Test Method and Test Setup

As presented in Photo 1(a), all the specimens were tested using a high-stiffness, high-capacity (58,800kN) compression testing machine. This unique device has the capacity and stiffness required for performing such tests. The machine is also equipped with a sophisticated servo-control and data acquisition system, presented in Photo 1(b) and Photo 1(c).

The test procedure follows the ASTM C39 standard [19] and the strain rate in the tests was 25micro-strain/sec. The acquired data includes the applied axial load, P, the axial deformation of concrete, and the transverse and axial strain of the FRP jacket. As presented in Photo 2, the axial deformation in the middle portion of the concrete was measured with a gauge length of $H/2$, using a linear potentiometer, to obtain data that are unaffected by potentially imperfect contacts or end confinement due to the friction between the ends of the specimen and the loading platens. The jacket strains were measured using electrical resistance gauges with a gauge length of 10mm.

3.3 Experimental Results

Table 3 presents the test results of the CFRP confined square concrete columns. In general, the compressive strength and ultimate strain of the square concrete columns with a particular CFRP volumetric ratio decline as the column side to corner radius ratio (D/r) increases. For instance, in Table 3, the compressive strengths of the specimens with $\rho_j = 0.5\%$ decline from 44.36MPa and 40.87MPa (S15-DR05-C2-200-1, S15- DR05-C2-200-2) to 30.17MPa and 29.21MPa (S45- DR15-C4-300-1, S45-DR15-C4-300-2), as their D/r ratios increase from 5 to 15. The ultimate axial strains of the square concrete columns decline from 1.89% and 1.56% to 1.31% and 1.33%, respectively.

Table 4 presents the test results for FRP confined rectangular concrete columns. The compressive strengths of rectangular concrete columns with a given CFRP volumetric ratio ($\rho_j = 1.0\%$) and column side to corner radius ratio ($D/r = 10$), decline as the column side aspect ratio (B/D) increases. For instance, in Table 4, the compressive strength of specimens with $\rho_j = 1.0\%$ and $D/r = 10$ decline from 33.23MPa and 34.81MPa (R30-BD1.5-DR10-C6-300-1, R30-BD1.5-DR10-C6-300-2) to 31.15MPa and 28.80MPa as their B/D ratios increase from 1.5 to 2. Simultaneously, the ultimate axial strains of the specimens decline from 1.52 and 1.56% to 1.43%.



(a) High-capacity testing machine



(b) Computer control system



(c) Data acquisition system

Photo 1 Compression testing machine at Lien-Foo pillar plastic Inc.



(a) Square columns



(b) Rectangular columns

Photo 2 Test and instrumentation configurations

4. COMPARISON WITH EXPERIMENTAL RESULTS

4.1 Tests by Rochette *et al.* [20]

Tests were performed on 13 500mm-high concrete specimens with square section. The specimens had 152 × 152mm sides with various corner radii and were wrapped in three, four or five carbon plies. The mechanical properties of the composites were E_j = 82.7GPa, ε_{ult} = 1.5%, t_j = 0.30mm and w = 1.8g/cm^3. The properties of the unconfined concrete were f'_{co} = 42.0MPa, ε_{co} = 0.002, E_c = 32,400MPa and ν = 0.2.

Table 2 presents the experimental results and those of the nonlinear FEM analyses. The differences between the normalized compressive strengths in the test results and those obtained using the proposed models are –0.17, 1.41, 4.46 and 8.61% for specimens C100-C2, S38-C3, S25-C3 and S5-C3, respectively. Simultaneously, the differences between the ultimate axial strains for these specimens are –2.67, 0.34, 0.90 and –4.05%. Figure 8 compares the test results with the analytical axial stress versus axial strain. The consistency between the results obtained using the proposed nonlinear finite element results (solid lines) and in the test (markers) is quite satisfactory.

4.2 Tests in this Investigation

Tables 3 and 4 presents the experimental results and the analytical results. The differences between the normalized compressive strengths from the test results and those obtained using the proposed models are small - except for those of four specimens (S15-DR05-C2-200-2, S30-DR10-C3-250-1, R15-BD1.5-DR05-C2-250-2 and R15-BD2.0-DR05-C4-250-1), which have

https://doi.org/10.1017/jmech.2012.118 Published online by Cambridge University Press

Table 2 Comparisons between tests [17] and results of nonlinear finite element model for FRP confined square concrete columns

Specimen	Dimension (mm)	f'_{cc}/f'_{co} (Experiment)	f'_{cc}/f'_{co} (NFEM)	Error (%)	ε_{cu} (%) (Experiment)	ε_{cu} (%) (NFEM)	Error (%)
C100-C2	152 × 152	1.75	1.747	–0.17	1.57	1.528	–2.67
S38-C3	152 × 152	1.20	1.217	1.41	1.16	1.164	0.34
S25-C3	152 × 152	1.03	1.076	4.46	0.89	0.898	0.90
S5-C3	152 × 152	0.94	1.021	8.61	0.69	0.662	–4.05

Table 3 The error analysis of FRP confined square concrete columns between nonlinear finite element model and experimental results

Specimen No.	Dimension (mm)	ρ_j (%)	f'_{cc} (MPa)	f'_{cc}/f'_{co} (Exp.)	f'_{cc}/f'_{co} (NFEM)	Error (%)	ε_{cu} (%) (Exp.)	ε_{cu} (%) (NFEM)	Error (%)
S15-DR05-C2-200-1	150 × 150 × 300	0.56	44.36	2.15	2.19	1.89	1.89	1.92	1.48
S15-DR05-C2-200-2	150 × 150 × 300	0.56	40.87	1.98	2.19	10.61	1.56	1.92	23.09
S15-DR05-C3-250-1	150 × 150 × 300	1.04	55.78	2.71	2.88	6.52	2.33	2.35	0.85
S15-DR05-C3-250-2	150 × 150 × 300	1.04	57.03	2.77	2.88	4.18	2.30	2.35	2.02
S30-DR10-C3-250-1	300 × 300 × 600	0.53	31.56	1.53	1.71	11.36	1.20	1.49	24.24
S30-DR10-C3-250-2	300 × 300 × 600	0.53	33.72	1.64	1.71	4.21	1.53	1.49	–3.04
S30-DR10-C5-300-1	300 × 300 × 600	1.06	42.84	2.08	2.18	4.65	1.78	1.81	1.72
S30-DR10-C5-300-2	300 × 300 × 600	1.06	40.90	1.99	2.18	9.61	1.91	1.81	–5.58
S45-DR15-C4-300-1	450 × 450 × 900	0.57	30.17	1.46	1.52	3.77	1.31	1.35	2.54
S45-DR15-C4-300-2	450 × 450 × 900	0.57	29.21	1.42	1.52	7.19	1.33	1.35	1.29
S45-DR15-C7-300-1	450 × 450 × 900	1.00	34.32	1.67	1.80	8.08	1.53	1.55	1.66
S45-DR15-C7-300-2	450 × 450 × 900	1.00	36.45	1.77	1.80	1.75	1.60	1.55	–3.26

Table 4 The error analysis of FRP confined rectangular concrete columns between nonlinear finite element model and experimental results

Specimen No.	Dimension (mm)	ρ_j (%)	f'_{cc} (MPa)	f'_{cc}/f'_{co} (Exp.)	f'_{cc}/f'_{co} (NFEM)	Error (%)	ε_{cu} (%) (Exp.)	ε_{cu} (%) (NFEM)	Error (%)
R15-BD1.5-DR05-C2-250-1	150 × 225 × 450	0.58	36.76	1.78	1.83	2.53	1.65	1.69	2.21
R15-BD1.5-DR05-C2-250-2	150 × 225 × 450	0.58	35.09	1.70	1.83	7.41	1.22	1.69	38.37
R15-BD1.5-DR05-C3-300-1	150 × 225 × 450	1.05	45.14	2.19	2.22	1.35	1.94	2.02	4.01
R15-BD1.5-DR05-C3-300-2	150 × 225 × 450	1.05	44.58	2.16	2.22	2.63	2.00	2.02	0.90
R30-BD1.5-DR10-C3-300-1	300 × 450 × 900	0.53	29.55	1.43	1.45	0.89	1.31	1.33	1.43
R30-BD1.5-DR10-C3-300-2	300 × 450 × 900	0.53	28.48	1.38	1.45	4.67	1.37	1.33	–3.39
R30-BD1.5-DR10-C6-300-1	300 × 450 × 900	1.07	33.23	1.61	1.72	6.44	1.52	1.58	4.41
R30-BD1.5-DR10-C6-300-2	300 × 450 × 900	1.07	34.81	1.69	1.72	1.62	1.56	1.58	1.39
R15-BD2.0-DR05-C2-250-1	150 × 300 × 600	0.53	32.15	1.56	1.60	2.52	1.47	1.50	1.79
R15-BD2.0-DR05-C2-250-2	150 × 300 × 600	0.53	31.57	1.53	1.60	4.42	1.43	1.50	5.04
R15-BD2.0-DR05-C4-250-1	150 × 300 × 600	1.06	36.86	1.79	1.93	7.74	1.52	1.82	20.16
R15-BD2.0-DR05-C4-250-2	150 × 300 × 600	1.06	35.87	1.74	1.93	10.74	1.76	1.82	3.64
R30-BD2.0-DR10-C4-250-1	300 × 600 × 1200	0.54	26.99	1.31	1.33	1.19	1.20	1.24	3.43
R30-BD2.0-DR10-C4-250-2	300 × 600 × 1200	0.54	25.42	1.23	1.33	7.44	1.26	1.24	–1.69
R30-BD2.0-DR10-C8-250-1	300 × 600 × 1200	1.07	31.15	1.51	1.52	0.60	1.43	1.45	1.27
R30-BD2.0-DR10-C8-250-2	300 × 600 × 1200	1.07	28.80	1.40	1.52	8.82	1.60	1.45	–8.98

lower compressive strength and ultimate strain due to earlier carbon fiber breakage by sharp aggregate at corner of concrete column. The ultimate axial strains predicted using the proposed models are also very satisfactory. Details of the comparisons follow.

4.3 Effect of Column Side Aspect Ratio (B/D)

Figures 9(a) and 9(b) plot the effects of the side aspect ratio (B/D) on the compressive strength and ultimate strain of the CFRP confined rectangular concrete columns of fixed CFRP volumetric ratio (1.0%). The agreement between the nonlinear finite element results (solid lines) and the experimental results (markers) is excellent. The figures also indicate that for columns with the same side to corner radius ratio (D/r = 5, 10), the normalized compressive strength and ultimate axial strain decline as the column side aspect ratio (B/D) increases.

4.4 Effect of Column Side to Corner Radius Ratio (D/r)

Figures 10(a) and 10(b) plot the effects of column side to corner radius ratio (D/r) on the compressive strength and ultimate strain of the CFRP confined

https://doi.org/10.1017/jmech.2012.118 Published online by Cambridge University Press

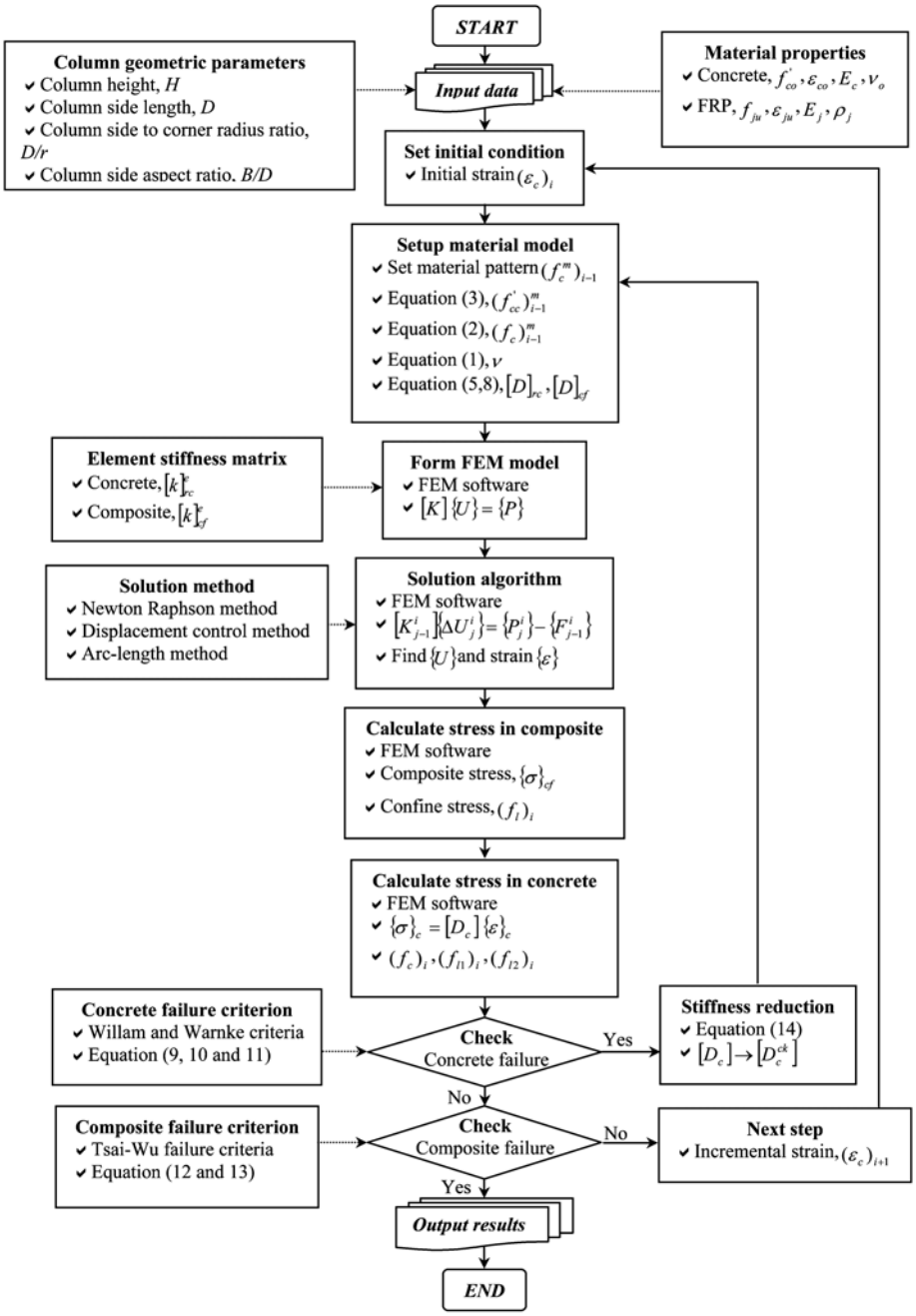


Fig. 7 Analysis flowchart of FRP confined rectangular concrete column nonlinear finite element model

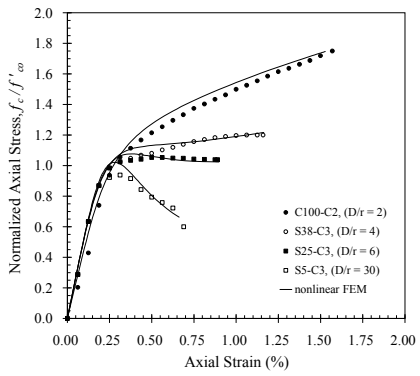


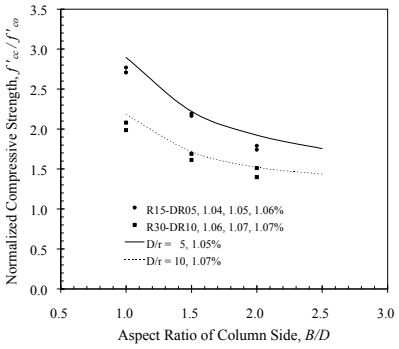
Fig. 8 Comparisons between tests [17] and analyses for axial stress versus axial strain

square concrete columns of fixed CFRP volumetric ratio (0.5 and 1.0%). The normalized compressive strength and ultimate axial strain decline as the column side to corner radius ratio (D/r) increase, and the agreement between the nonlinear finite element results (solid lines) and the experimental results (markers) is also satisfactory.

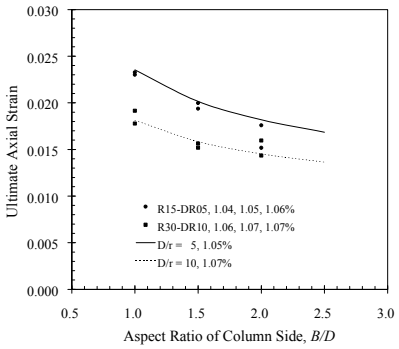
4.5 Effect of CFRP Volumetric Ratio

Figures 11(a) and 11(b) plot the effects of CFRP volumetric ratio on the compressive strength and ultimate strain of confined square concrete columns of fixed column side to corner radius ratio (D/r = 5, 10 and 15). The agreement between the nonlinear finite element results (solid lines) and the experimental results (markers) is quite good. Figure 11 also indicates that

https://doi.org/10.1017/jmech.2012.118 Published online by Cambridge University Press

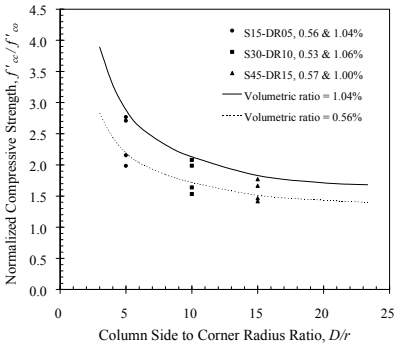


(a)

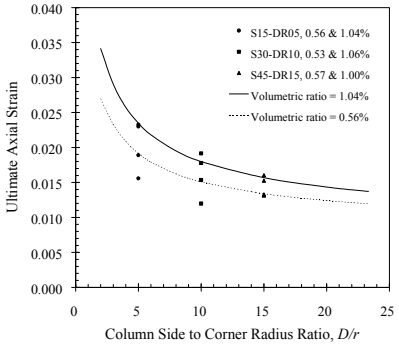


(b)

Fig. 9 Comparisons for effect of column side aspect ratio (B/D) on (a) normalized compressive strength and (b) ultimate axial strain between experiment and analysis results for columns with $\rho_j = 1.05\%$

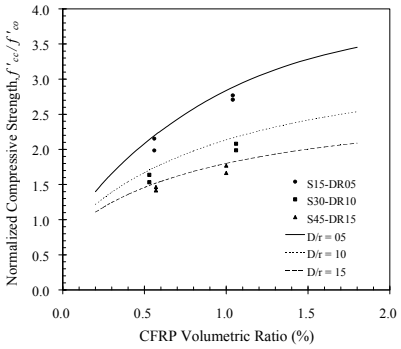


(a)

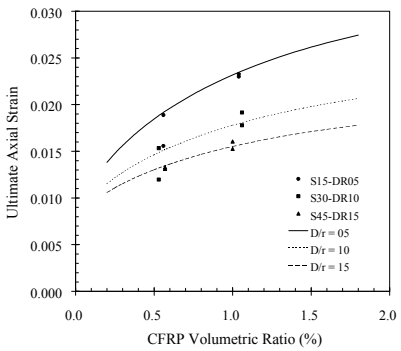


(b)

Fig. 10 Comparisons for effect of column side to corner radius ratio (D/r) on (a) normalized compressive strength and (b) ultimate axial strain between experiment and analysis results for columns with $B/D = 1$



(a)



(b)

Fig. 11 Comparisons for effect of CFRP volumetric ratio (ρ_j) on (a) normalized compressive strength and (b) ultimate axial strain between experiment and analysis results for columns with $B/D = 1$

for columns of a given side to corner radius ratio (D/r = 5, 10 and 15), the normalized compressive strength and ultimate axial strain increase with the CFRP volumetric ratio.

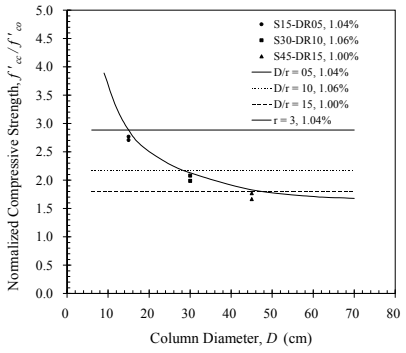
4.6 Effect of Column Size (D)

Figures 12 and 13 plot the effects of column size (D) on the compressive strength and ultimate axial strain of the CFRP confined rectangular concrete columns of fixed CFRP volumetric ratio (1.0%). For columns of a given corner radius ($r = 3$), the normalized compressive strength and ultimate axial strain decline as the column size increases. However, size does not affect the normalized compressive strength or ultimate axial strain of columns of a particular CFRP volumetric ratio and column side to corner radius ratio (D/r). Figures 12 and 13 indicate that the consistency between the nonlinear finite element results (solid lines) and the experimental results (markers) is satisfactory.

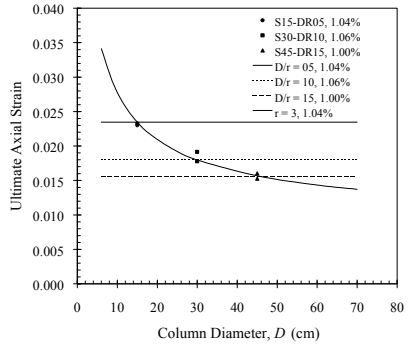
5. PARAMETRIC STUDY

The parametric study considers three factors. They are column size, reinforcing CFRP volumetric ratio and column side to corner radius ratio (D/r). The range of column side lengths considered is 20 to 200cm; the range of CFRP volumetric ratios is 0.0 to 3.0% and the range of column side to corner radius ratios is 2 to 60.

https://doi.org/10.1017/jmech.2012.118 Published online by Cambridge University Press

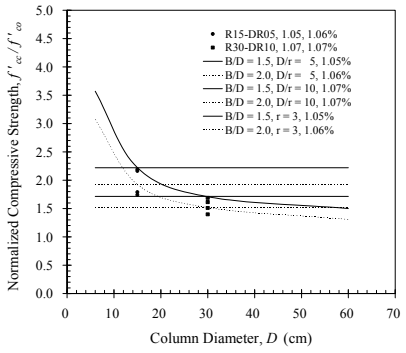


(a)

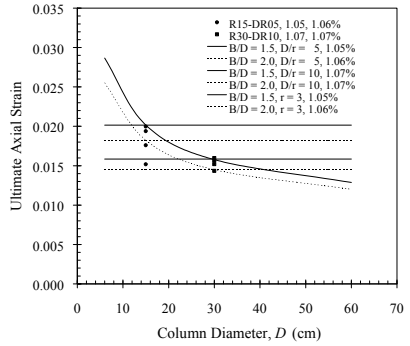


(b)

Fig. 12 Comparisons for effect of column size (D) on (a) normalized compressive strength and (b) ultimate axial strain between experiment and analysis results for columns with B/D = 1 and ρ_j = 1.05%



(a)



(b)

Fig. 13 Comparisons for effect of column size (D) on (a) normalized compressive strength and (b) ultimate axial strain between experiment and analysis results for columns with ρ_j = 1.05%

The plain concrete strength in all cases is 27.47MPa (280kgf/cm^2). The CFRP properties are E_j = 230.54GPa, f_{ju} = 1,152.67MPa, ε_{ju} = 0.005 and t_j = 0.1375mm/layer (FAW 250).

5.1 Effect of Column Side Aspect Ratio (B/D)

The effects of column side aspect ratio (B/D) on the compressive strength and ultimate strain of the CFRP confined rectangular concrete columns of fixed plain concrete strength (27.47MPa) and column side to corner radius ratio (D/r = 10) are investigated. Figure 14 plots the results of parametric study. The figure indicates that, for rectangular columns of a particular CFRP volumetric ratio (0.1, 0.5, 1.0, 2.0 and 3.0%), the normalized compressive strength decreases rapidly as the column side aspect ratio (B/D) increases. Simultaneously, the ultimate axial strain of rectangular concrete columns decreases as the column side aspect ratio (B/D) increases, as presented in Fig. 14(b).

5.2 Effect of Column Side to Corner Radius Ratio (D/r)

The effects of the column side to corner radius (D/r) of columns of fixed plain concrete strength (27.47MPa) and column side aspect ratio (B/D = 1) on the compressive strength and ultimate strain of the CFRP confined square concrete columns are examined. Figure 15 presents the results of the parametric study. Figure 15(a) reveals that the normalized compressive strength of square concrete columns for a particular CFRP volumetric ratio (0.1, 0.5, 1.0, 2.0 and 3.0%) falls rapidly as the column side to corner radius ratio (D/r) increases, while the ultimate axial strain of such columns also falls as presented in Fig. 15(b).

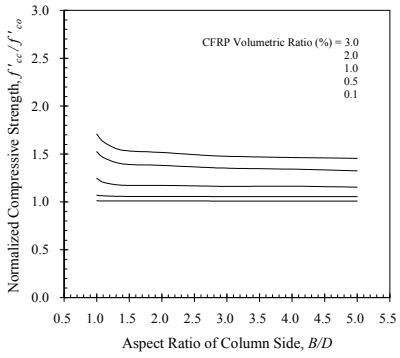
5.3 Effect of CFRP Volumetric Ratio (ρ_j)

The effects of the CFRP volumetric ratio (ρ_j) on the compressive strength and ultimate strain of the CFRP confined square concrete columns of fixed plain concrete strength (27.47MPa) and column side aspect ratio (B/D = 1) are studied. Figure 16 plots the results of the parametric study. As presented in Fig. 16(a), the normalized compressive strength of square concrete columns of a particular column side to corner radius ratio (D/r = 2, 4, 10, 20 and 30) increases with CFRP volumetric ratio. Simultaneously, the ultimate axial strain of square concrete columns increases with the CFRP volumetric ratio as presented in Fig. 16(b).

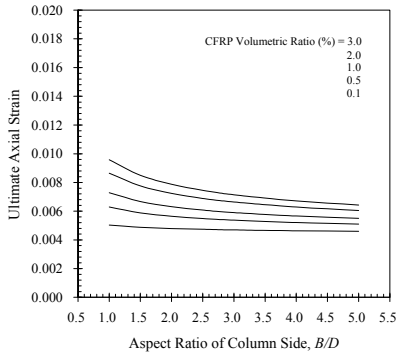
5.4 Effect of Column Size (D)

The effects of column size on the compressive strength and ultimate axial strain of the CFRP confined square concrete columns of equal plain concrete strength (27.47MPa) and column side aspect ratio (B/D = 1) are investigated. Figure 17 plots the results of the parametric study. As shown in Fig. 17(a), the normalized compressive strength of square concrete columns with a given corner radius (r = 3, 5 and 10) and CFRP

https://doi.org/10.1017/jmech.2012.118 Published online by Cambridge University Press

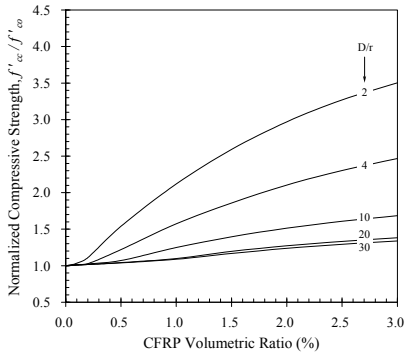


(a)

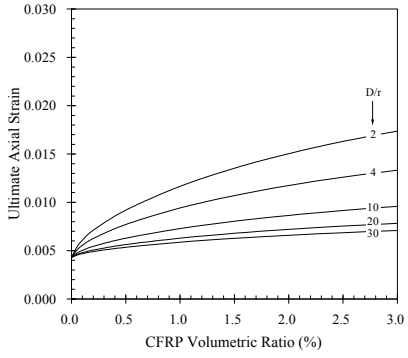


(b)

Fig. 14 Effect of column side aspect ratio (B/D) on (a) normalized compressive strength and (b) ultimate axial strain for columns with D/r = 10 and f'_{co} = 27.47MPa

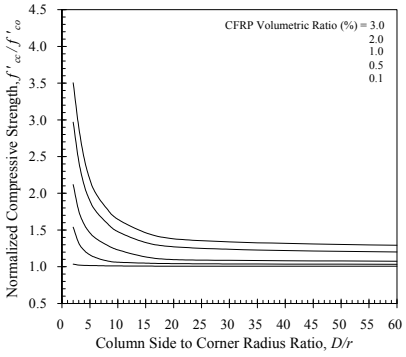


(a)

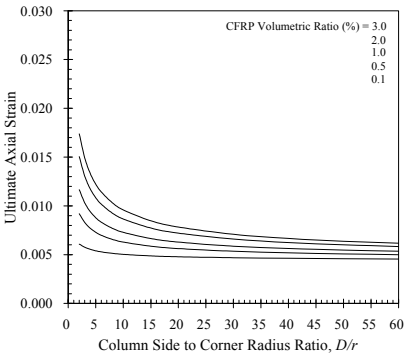


(b)

Fig. 16 Effect of CFRP volumetric ratio (ρ_j) on (a) normalized compressive strength and (b) ultimate axial strain for columns with B/D = 1 and f'_{co} = 27.47MPa

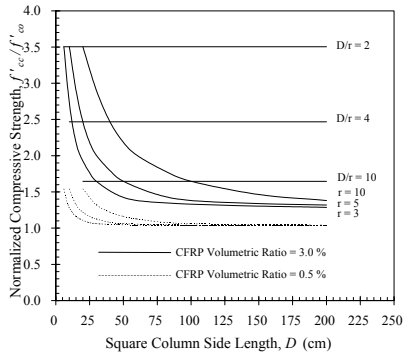


(a)

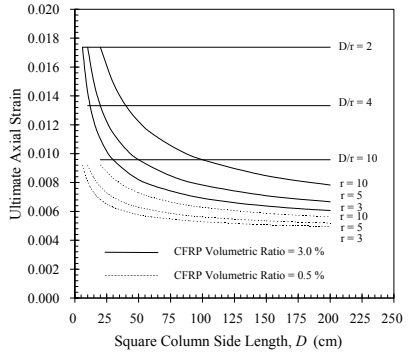


(b)

Fig. 15 Effect of column side to corner radius ratio (D/r) on (a) normalized compressive strength and (b) ultimate axial strain for columns with B/D = 1 and f'_{co} = 27.47MPa



(a)



(b)

Fig. 17 Effect of column size (D) on (a) normalized compressive strength and (b) ultimate axial strain for columns with B/D = 1 and f'_{co} = 27.47MPa

https://doi.org/10.1017/jmech.2012.118 Published online by Cambridge University Press

volumetric ratio (0.5 and 3.0%) declines as the column size increases. Similarly, as shown in Fig. 17(b), the ultimate axial strain of square concrete columns with a given corner radius and CFRP volumetric ratio declines as the column size increases. However, column size has no effects on normalized compressive strength and ultimate axial strain of columns with a given CFRP volumetric ratio and column side to corner radius ratio (D/r).

6. CONCLUDING REMARKS

The following conclusions are drawn regarding the effects of column size (D), CFRP volumetric ratio (ρ_j), column side to corner radius ratio (D/r) and column side aspect ratio (B/D) on the strength and ultimate strain of CFRP confined rectangular concrete columns.

1. The normalized column axial strength and ultimate strain increase with CFRP volumetric ratio (ρ_j), but decline as the column side to corner radius ratio (D/r) and column side aspect ratio (B/D) increase.
2. The normalized column axial strength and ultimate strain for columns of a particular corner radius (r) and CFRP volumetric ratio (ρ_j) fall as column size (D) increase.
3. Column size has no effect on normalized strength and ultimate strain of columns with a given CFRP volumetric ratio (ρ_j), column side to corner radius ratio (D/r) and column side aspect ratio (B/D).

For better confinement efficiency of the CFRP confined rectangular concrete columns, it is suggested that:

1. For the retrofitting of rectangular concrete columns for strength, more favorable column side aspect ratio (B/D) is less than or equal to 1.5, corner radius ratio (D/r) is less than or equal to 20 and CFRP volumetric ratio (ρ_j) is at least 0.5%.
2. For the retrofitting of rectangular concrete columns for ultimate strain, the preferred column side aspect ratio (B/D) is less than or equal to 3.0 and corner radius ratio (D/r) is less than or equal to 30; the CFRP volumetric ratio (ρ_j) can take any value.

Increasing the CFRP volumetric ratio (ρ_j) is the most effective approach for retrofitting rectangular concrete columns for buildings and bridges without any shape change (as when rectangular sections become elliptical, for example), but sometimes it is not practical and is costs too much.

ACKNOWLEDGEMENTS

The authors would like to thank the National Science Council of the Republic of China, Taiwan, for financially supporting this research under Contract No. NSC 89-2625-Z-002-067.

REFERENCES

1. Chang, K. C., Chang, S. P. and Liu, K. Y., "Seismic Retrofit Study of Rectangular RC Columns Lap Spliced at Plastic Hinge Zone," *Proceeding of 16th KKCNN Symposium on Civil Engineering*, Gyeongju, Korea, pp. 221–227 (2003).
2. Li, Y. F. and Sung, Y. Y., "Seismic Repair and Rehabilitation of a Shear-Failure Damaged Circular Bridge Column Using Carbon Fiber Reinforced Plastic Jacketing," *Canadian Journal of Civil Engineering*, **30**, pp. 819–829 (2003).
3. Li, Y. F. and Sung, Y. Y., "A Study on the Shear-failure of Circular Sectioned Bridge Column Retrofitted by Using CFRP Jacketing," *Journal of Reinforced Plastics and Composites*, **23**, pp. 811–830 (2004).
4. Vivo, L. D. and Rosati, L., "Ultimate Strength Analysis of Reinforced Concrete Section Subject to Axial Force and Biaxial Bending," *Computer Methods in Applied Mechanics and Engineering*, **166**, pp. 261–287 (1998).
5. Luccioni, B. M. and Rougier, V. C., "A Plastic Damage Approach for Confined Concrete," *Computers & Structures*, **83**, pp. 2238–2256 (2005).
6. Yeh, F. Y. and Chang, K. C., "Confinement Efficiency and Size Effect of FRP Confined Circular Concrete Columns," *Structural Engineering and Mechanics*, **26**, pp. 127–150 (2007).
7. Montoya, E., Vecchio, F. J. and Sheikh, S. A., "Numerical Evaluation of the Behaviour of Steel- and FRP-confined Concrete Columns Using Compression Field Modeling," *Engineering Structures*, **26**, pp. 1535–1545 (2004).
8. Wu, Y. F. and Wei, Y. Y., "Effect of Cross-Sectional Aspect Ratio on the Strength of CFRP-Confined Rectangular Concrete Columns," *Engineering Structures*, **32**, pp. 32–45 (2010).
9. Barrington, J., Dickson, D., Bisby, L. and Stratford, T., "Strain Development and Hoop Strain Efficiency in FRP Confined Square Columns," *American Concrete Institute, ACI Special Publication*, **1**, SP, pp. 147–166 (2011).
10. Elsanadedy, H. M., Al-Salloum, Y. A., Alsayed, S. H. and Iqbal, R. A., "Experimental and Numerical Investigation of Size Effects in FRP-Wrapped Concrete Columns," *Construction and Building Materials*, **29**, pp. 56–72 (2012).
11. Kupfer, H., Hilsdrof, H. K. and Rusch, H., "Behavior of Concrete Under Biaxial Stresses," *Journal of American Concrete Institute*, **66**, pp. 656–666 (1969).
12. Mander, J. B., Priestley, M. J. N. and Park, R., "Theoretical Stress Strain Model for Confined Concrete," *Journal of Structural Engineering*, ASCE, **114**, pp. 1804–1826 (1988).
13. Chang, G. A. and Mander, J. B., "Seismic Energy Based Fatigue Damage Analysis of Bridge Columns: Part I – Evaluation of Seismic Capacity," *Technical Report NCEER-94-0006, NCEER*, State University of New York, Buffalo, N.Y., pp. 3-32–3-34 (1994).
14. Yunus, S. M. and Kohnke, P. C., "An Efficient Through-Thickness Integration Scheme in an Unlimited Layer Doubly Curved Isoparametric Composite Shell Element," *International Journal for Numerical*

https://doi.org/10.1017/jmech.2012.118 Published online by Cambridge University Press

Numerical Methods in Engineering, **28**, pp. 2777–2793 (1989).
15. Willam, K. J. and Warnke, E. P., "Constitutive Model for the Triaxial Behavior of Concrete," *Proceeding of the International Association for Bridge and Structural Engineering*, **19**, pp. 1–30 (1975).
16. Tsai, S. W. and Hahn, H. T., *Introduction to Composite Materials*, Section 7.2, Technomic Publishing Company (1980).
17. Tsai, S. W., *Composites Design*, Third Edition, Section 11.6, Think Composites, Dayton, Ohio (1987).
18. ABAQUS, Inc., *ABAQUS Theory Manual and Analysis User's Manual*, Version 6.5, Providence, Rhode Island (2005).
19. ASTM C39, *Standard Test Method for Compressive Strength of Cylindrical Specimens*, Annual book of ASTM Standards 2005, Vol. 04.02, American Society for Testing Materials, West Conshohocken, PA.
20. Rochette, P. and Labossiere, P., "Axial Testing of Rectangular Column Models Confined with Composites," *Journal of Composites for Construction*, **4**, pp. 129–136 (2000).

(Manuscript received October 18, 2011,
accepted for publication May 21, 2012.)

https://doi.org/10.1017/jmech.2012.118 Published online by Cambridge University Press